J Mater Sci (2008) 43:5430–5435
DOI 10.1007/s10853-008-2845-1

Oxidation refining of iron using plasma-arc melting

Masahito Uchikoshi · Kazuki Imai · Kouji Mimura · Minoru Isshiki

Received: 31 January 2008 / Accepted: 30 June 2008 / Published online: 18 July 2008

Abstract Oxidation refining of Fe using plasma arc melting, by the addition of iron oxide as an oxidizing agent, has been carried out. In this refining process, an impurity element which has higher affinity for oxygen than iron was expected to be eliminated. As the result, decreases in Si, Mn, Al, Ca, Ga, and Zr were observed and 99.996 mass% of iron could be obtained from 99.93 mass% of electrolytic iron by plasma arc melting under oxidizing conditions followed by argon–hydrogen plasma arc melting. Specifically, the removal of Si was found to proceed by the distribution between in the liquid Fe phase and in the oxide phase. In addition, the relation of Si and oxygen concentration in liquid iron was consistent with the data in the literature.

Introduction

Recent remarkable development of advanced electronics industry requires higher purity materials. β-$FeSi_2$ is, for example, expected to be a new optical device [1] and it has been reported that the high quality epitaxial film grew on hydrogen terminated Si (111) substrate [2]. Under these circumstances, the demand for high purity Fe has increased as a constituent element of this compound semiconductor.

The commercial high purity Fe is manufactured mainly by electrolysis [3–5]. However, the current purity of these Fe is still 99.9 mass% including gaseous impurities, and far from the semiconductor level. Therefore, a simple and effective refining process of Fe has been required.

Purification process of metals generally consists of several steps involving either hydrometallurgical and pyrometallurgical techniques. However, a risk of contamination increases with an increase in the number of refining steps. The fewer steps are desirable for the purification processes. In most cases, the melting process must be used as the final step. Therefore, removing as many impurities as possible is required for the melting process.

There are the various melting methods, such as electron beam melting and induction melting. Among these methods, plasma-arc melting (referred as PAM, hereafter) has been recognized to be efficient for refining and degassing of several metals, when hydrogen is added to the plasma generating gas. For example, deoxidation of Fe, Co, and Ta [6–8]; decarburization of Fe [7]; and removal of metallic impurities from Zr, Ta, and Fe [9–14] have been reported. On the contrary, there have been few reports dealing with oxidation refining of Fe using PAM [15].

In the case of oxidation refining, two useful refining effects are anticipated, as follows.

1. An impurity element evaporates from the surface of a molten metal as the suboxide having a higher vapor pressure than the liquid Fe.
2. An impurity element distributes in the oxide phase rather than in the liquid Fe phase.

Figure 1 shows the formation of various metal oxides as functions of p_{O_2} and temperature [16], and it is understood that many impurities in Fe have stronger affinities than Fe. So, these elements are supposed to be eliminated through the refining effect 1 or 2.

Although oxidation refining is implemented widely in industry, represented by the steel converter, it generally

M. Uchikoshi (✉) · K. Mimura · M. Isshiki
Institute of Multidisciplinary Research for Advanced Materials, Tohoku University, 2-1-1, Katahira, Aoba-ku, Sendai 980-8577, Japan
e-mail: hpm@tagen.tohoku.ac.jp

K. Imai
Tohoku University, Sendai, Japan

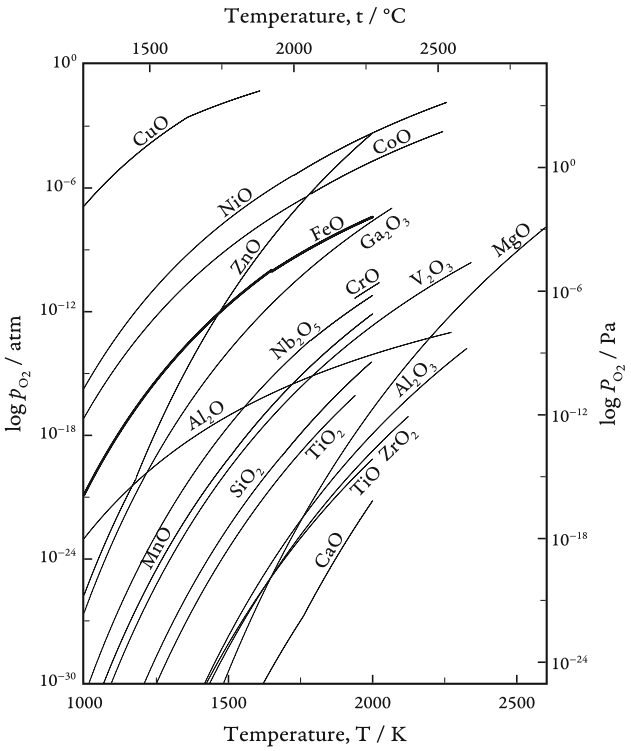

Fig. 1 Formation of various oxides (MO_x) relating to p_{O_2} and temperature

takes a long time to attain equilibrium [17–21]. In addition, because the crucible is made of refractory materials, the molten metal is subject to contamination from the crucible. Rapid reactions due to vigorous convection and less contamination from water-cooled Cu crucible are the advantages of PAM against the typical oxidation refining.

Nevertheless, a large amount of oxygen remains in Fe through oxidation refining. H_2–Ar PAM is very available for reducing the residual large amount of oxygen to a low level [7]. Consequently, oxidation refining using PAM followed by H_2–Ar PAM is expected to be a useful refining technique.

In the present work, a commercial electrolytic Fe with 99.9 mass% was treated by the oxidation refining using PAM to confirm the refining efficiency of the process. Fe–Si alloys were also treated to examine the kinetics of removing Si.

Experimental procedure

The plasma arc melting furnace in a laboratory scale, the details of which was published in a previous report [13], was used in this work. The plasma torch is a D. C. arc discharged type with a maximum power of 20 kW. A thoriated W cathode was mounted in the plasma torch and a specimen placed on a water-cooled copper crucible was utilized as an anode. High-purity Ar (greater than 99.9995%) and H_2 (greater than 99.9999%) were used as the plasma generating gas and the experiment was carried out under an atmospheric pressure. In the case of H_2–Ar PAM, the content of H_2 in plasma generating gas was fixed at 10 vol.%. The specimen was turned upside down and melted again for the same time for homogenization after melting for certain time, thus the total melting time was expressed as the sum of both the times.

Figure 2 shows the flow chart of the experiment. Two types of samples were tested in this work. One is the electrolytic 99.9 mass% Fe and the other is Fe–Si alloy (Si = 540 ± 30 mass ppm). The electrolytic Fe was used for the evaluation of refining efficiency by oxidation refining using Ar PAM followed by H_2–Ar PAM. Fe–Si alloy, which was prepared by melting the electrolytic Fe and the high-purity Si, was used for examining the kinetics of removal of Si by oxidation refining using Ar PAM.

Dembovsky [15] has reported the decarburization of Fe by PAM in Ar–O_2 atmosphere, which is a slag-free process. In the present work, a slag composed of Fe-oxide was formed to enhance the effect of oxidation refining using Ar PAM. The solubility limit of oxygen in Fe at the melting point is reported to be about 0.19 mass% [22] and the equilibrium constant can be written as follows:

$$\log[\text{mass\%O}]X_{\text{Fe}} = -\frac{5909}{T} + 2.516 \quad (1)$$

where [mass%O] and X_{Fe} represents a solubility limit of oxygen and a mole fraction of Fe, respectively. T indicates absolute temperature. In this melting process, an amount of oxygen over the solubility limit was added to form

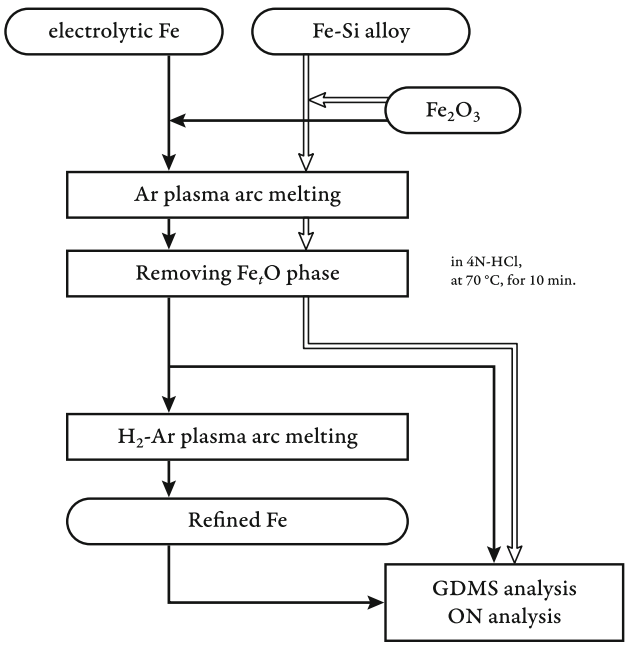

Fig. 2 Flow chart of the experiment

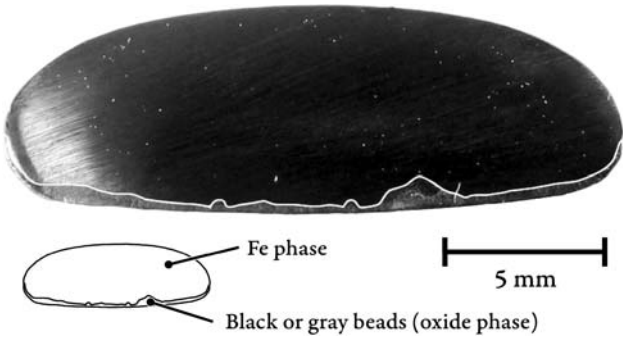

Fig. 3 Cross sectional view of the specimen melted by oxidation refining using Ar PAM

Fe-oxide phase, and Fe_2O_3 was added as an oxidant. The electrolytic Fe and Fe–Si alloys mixed with 2–7.5 mass% of Fe_2O_3, which corresponds to 0.6–2.3 mass% of oxygen, was melted by Ar PAM.

After solidification, some black or gray beads were observed at the bottom of the specimen, as shown in Fig. 3. Cross sectional areas of black or gray beads were characterized by electron probe X-ray microanalysis, EPMA. The concentrations of the metallic impurities in Fe were analyzed by glow discharge mass spectrometry, GDMS. The concentrations of oxygen were also analyzed by the inert gas fusion-infrared spectroscopic method using LECO TC-436.

Then 10 vol.%H_2–Ar PAM for 3.6 ks (60 min) was employed to the electrolytic Fe after removing oxidized scale with 2M-HCl acid solution at 70 °C for 600 s (10 min) to evaluate the total refining efficiency.

The flow rate of plasma generating gas was 8.3×10^{-5} m^3 s^{-1} (5 dm^3 min^{-1}), and the melting power was 3 kW throughout the present work.

Results and discussion

Refining efficiency

Firstly, PAM of electrolytic Fe under oxidizing condition was carried out. In this case, the total melting time was fixed at 1.2 ks (20 min), but the added amount of Fe_2O_3 was varied. Table 1 shows the concentration of impurities in Fe. The elements in italics have a stronger affinity for oxygen than Fe; among these, the elements in boldface decreased by oxidation refining using Ar PAM. The high refining efficiency by oxidation refining using Ar PAM is evidenced by the increase in the purity of Fe. Furthermore, the combination of oxidation refining using Ar PAM and H_2–Ar PAM increased the purity of Fe from 99.93 mass% to 99.996 mass%.

After melting with the addition of Fe_2O_3, the concentrations of oxygen in Fe were constant at 0.19 mass%. This value corresponds to the solubility limit at the melting point, as reported by Tankins et al. [22].

The elements which have stronger affinity for oxygen than Fe were classified into three groups: (a) not decreased, (b) decreased by melting with the addition of Fe_2O_3, but not decreased without the addition of Fe_2O_3, (c) decreased by melting with and without the addition of Fe_2O_3. Ti, Cr, and Nb were classified into group (a). The concentration of these elements even in the starting material were very low, around 1 mass ppm. So, the reduction of them cannot be observed and it is not clear in this work whether oxidation refining using Ar PAM is effective for their elimination. The elements classified into group (b) were Si and Mn. A decrease in Si was observed clearly compared with Mn. In this case, the addition of Fe_2O_3 is necessary for eliminating Si and Mn. Al, Ca, Ga, and Zr were classified into group (c). Particularly, Ga and Zr decreased down to a few ten mass ppb. Since the starting material contained a few hundred mass ppm of oxygen, the formation of the oxides of several impurities in liquid Fe seems to be possible without the addition of Fe_2O_3.

A likely explanation is that the elements in group (c) form their suboxides and evaporate from liquid Fe. However, because the vapor pressure of their suboxides except Al_2O are very small [16], their evaporation are impossible. Hence, it is considered that the elements in group (c) form their oxides and these oxides are segregated from liquid Fe. But these oxides were not found after solidification. This is because the initial concentrations of these elements in group (c) are very small. Therefore, further examination is necessary to make it clear how these elements are removed.

Kinetics of removing Si

Among the tested impurities, elimination of Si is the most obvious and it was supposed to proceed by the distribution of Si between into the Fe-oxide and into the Fe phase. To investigate the behavior of Si, oxidation refining of Fe–Si alloy ($Si = 540 \pm 30$ mass ppm) using Ar PAM was examined. In this case, 2 mass% of Fe_2O_3 was added to Fe–Si alloy and the total melting time was varied up to 2.4 ks (40 min).

Figure 4 shows the change in the concentration of Si and the mass loss of the specimens as a function of total melting time. The concentration of Si decreased rapidly down to 3 mass ppm in 120 s (2 min) and then became stable at 8.5 mass ppm over 1.8 ks (30 min) melting. And the concentrations of oxygen in all specimens were consistently 0.165 mass%. But the decrease in the mass of specimen is proportional to the total melting time.

If the removal of Si would be caused by the evaporation of Si suboxide, the mass of the specimen must decrease through the evaporation of SiO. The mass loss derived from the difference in Si concentration between 540 and

Table 1 Change in the impurity concentrations analyzed by GDMS and LECO and the purity of Fe before and after the refining treatment

Element	Starting material	The added amounts of Fe_2O_3/mass%				Per mass ppm O-PAM[a] + H2-PAM
		0	2.5	5.0	7.5	
Al	5 ± 1	2	3	0.6	1	0.5
Si	7 ± 3	10	0.7	0.5	0.2	0.2
P	16 ± 2	11	12	13	12	7
S	23 ± 2	–	–	–	20	7
Cl[b]	(125 ± 75)	(13)	(6)	(5)	(3)	(1)
Ca	1	0.1	0.1	0.2	0.02	0.04
Ti	0.8	0.6	0.6	0.7	0.5	0.6
Cr	0.5 ± 0.3	0.3	0.4	0.7	0.6	0.4
Mn	1.5 ± 0.5	1	0.7	0.8	0.2	0.1
Co	3 ± 1	2	2	2	3	3
Ni	1.2 ± 0.8	0.3	0.4	0.6	1	1
Cu	1.5 ± 0.5	2	4	2	2	0.7
Zn	3.5 ± 0.5	0.1	0.05	0.05	0.08	0.08
Ga	1	0.05	0.02	0.05	0.1	0.05
Zr	0.3	0.03	0.005	0.001	0.002	0.001
Nb	0.3	0.3	0.3	0.3	0.3	0.3
Mo	1	1	1	1	1	1
O[c]	350 ± 50	200	1900	1900	1900	2
Purity of Fe/ mass%						
Excluding O	99.97 ± 0.01	99.994	99.996	99.996	99.994	99.996
Including O	99.93 ± 0.02	99.97	99.80	99.80	99.80	99.996

[a] O-PAM denotes oxidation refining using plasma arc melting

[b] The parenthetical values represent the ionic strengths, because the relative sensitivity coefficients of the elements were not available

[c] The concentration of O was analyzed by LECO

8.5 mass ppm is calculated to be about 0.083% when Si evaporated as SiO, and this value is indicated by a thin solid line in Fig. 4. But the mass loss was less than 0.0003% at the early melting stage. Therefore, the removal of Si cannot be explained by the evaporation of its sub-oxide. From this result, Si must have migrated to the oxide phase rather than to the Fe phase. Then, the distribution of Si should be explained as follows.

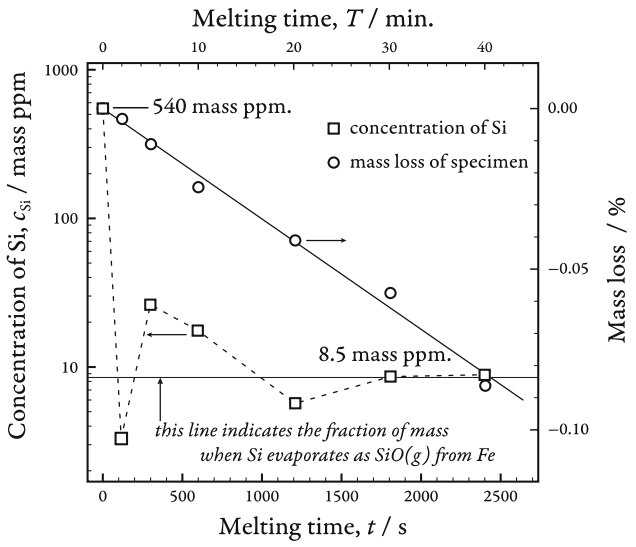

Fig. 4 Change in the concentration of Si as a function of total melting time

There have been many investigations on equilibrium between oxygen and several elements in liquid Fe from a viewpoint of the deoxidation of Fe. For example, the following chemical reaction, corresponding to deoxidation of liquid Fe with Si, has been reported [17–21, 23–25].

$$\underline{\mathrm{Si}} + 2\underline{\mathrm{O}} = \mathrm{SiO_2(s)} \tag{2}$$

where underline indicates the element dissolved in liquid Fe. The relation between the concentration of Si and oxygen is calculated by the following equation [24, 25].

$$\begin{aligned} &{}^{0}\Omega_{\mathrm{Fe-Si}} X_{\mathrm{Fe}}(1 - 3X_{\mathrm{Si}}) \\ &+ {}^{1}\Omega_{\mathrm{Fe-Si}} X_{\mathrm{Fe}}(X_{\mathrm{Fe}} - 2X_{\mathrm{Si}} - 6X_{\mathrm{Fe}}X_{\mathrm{Si}} + 6{X_{\mathrm{Si}}}^2) \\ &+ {}^{0}\Omega_{\mathrm{Fe-O}} X_{\mathrm{Fe}}(2 - 3X_{\mathrm{O}}) \\ &+ {}^{1}\Omega_{\mathrm{Fe-O}} 2X_{\mathrm{Fe}}(X_{\mathrm{Fe}} - 2X_{\mathrm{O}} - 3X_{\mathrm{Fe}}X_{\mathrm{O}} + 3{X_{\mathrm{O}}}^2) \\ &+ \Omega_{\mathrm{Si-O}}(2X_{\mathrm{Si}} + X_{\mathrm{O}} - 3X_{\mathrm{Si}}X_{\mathrm{O}}) \\ &+ \mathrm{R}T(\ln X_{\mathrm{Si}} + 2\ln X_{\mathrm{O}}) \\ &- \Delta G^{\circ}_{\mathrm{f,SiO_2}} = 0 \end{aligned} \tag{3}$$

where Ω and X are the interaction parameter and the mole fraction of elements indicated by its subscript, respectively [24, 25]. R is the molar gas constant and T is the absolute temperature. $\Delta G^{\circ}_{\mathrm{f,SiO_2}}$ is the Gibbs' free energy of SiO_2 formation [26]. The functions of Ω and $\Delta G^{\circ}_{\mathrm{f,SiO_2}}$ are listed

in Table 2 and they would be helpful to the thermodynamical consideration on the reaction of Eq. 2 in liquid Fe.

Hence, the relation between the concentration of Si and oxygen obtained in the present study are compared with the literature [17–21, 23–25, 27], as shown in Fig. 5. The lines are estimated based upon Eq. 3 [24, 25].

When the initial concentration of Si was 540 mass ppm, the results are in agreement with the reported data obtained near the melting point. Thus oxidation refining of Fe using Ar PAM is well illustrated by the equilibrated relationships represented by Eq. 3.

In addition, the concentration of oxygen in the electrolytic Fe was consistent with the value at the melting point described above, and the relation of Si and oxygen in Fe is also consistent with that represented by Eq. 3 near the melting point. Therefore, the temperature of the liquid Fe was estimated near the melting point, not exceeding it.

The results suggest that the concentration of Si and oxygen reached to the equilibrium in 1.8 ks (30 min) with Ar PAM in the present work, whereas it takes a few tens hours to reach the equilibrium with high-frequency induction heating as reported in the literature [17–21]. It is one of the advantages of PAM that the convection in a molten specimen makes the equilibrating time tremendously short.

Figure 6 shows the cross sectional SEM images of (a) black and (b) gray beads formed on the surface of specimens. Each phase in the beads was characterized by the composition analysis of EPMA. The phases indicated by A, B, and C in Fig. 6 are Fe, $Fe_{1-x}O \cdot SiO_2$, and $Fe_{1-x}O$, respectively. There also appears porosity in the columnar structure in Fig. 6b. This porosity is caused by that $Fe_{1-x}O \cdot SiO_2$ and $Fe_{1-x}O$ phases were chipped away during mechanical polishing.

The black bead is composed of $Fe_{1-x}O \cdot SiO_2$ single phase, and the gray beads had three phases, those are metallic Fe, $Fe_{1-x}O \cdot SiO_2$, and $Fe_{1-x}O$. In the gray beads, Fe phase exhibits columnar shape perpendicular on the lower surface and the phases composed of $Fe_{1-x}O \cdot SiO_2$ and $Fe_{1-x}O$ exist between metallic Fe phases.

Only black beads were observed on the specimen molten for 120 s (2 min), while the proportion of gray beads

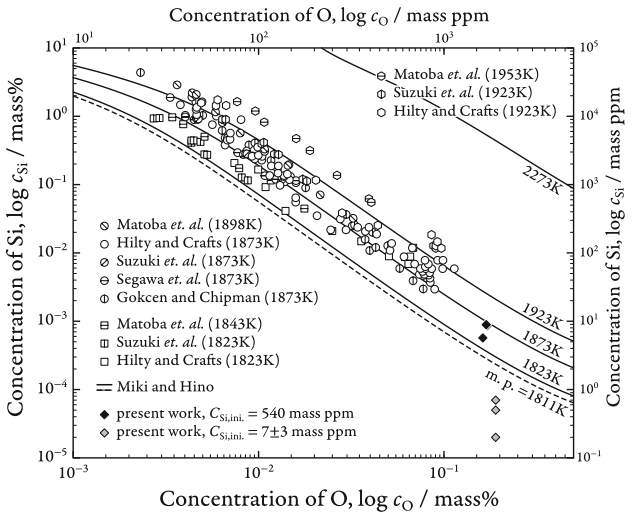

Fig. 5 Relation between Si and oxygen concentrations in liquid Fe. Lines are derived from Eq. 3 [24, 25]. $C_{Si,ini.}$ is the initial concentration of Si

increased with the increase in the total melting time. When the total melting time became longer than 1.8 ks (30 min), only gray beads were observed. Hence, almost all the Si was consumed to form $Fe_{1-x}O \cdot SiO_2$ single phase at the early melting stage, and then Si distributed between in the Fe phase and in the oxide phase following the equilibrium in liquid Fe represented by Eq. 3. This is the reason why the concentration of Si dropped and rose, then approached to the equilibrium as shown in Fig. 4.

Additionally, Si was decreased to less than 1 mass ppm when the electrolytic Fe, whose Si content was 7 ± 3 mass ppm, was melted by PAM under oxidizing condition. These values are notably lower than the calculated line at the melting point, as shown in Fig. 5. In a range in which the initial Si concentration is very low like 7 mass ppm listed in Table 1, the oxide phase seems to be attributed to removing Si as with the equilibrium between Si and oxygen in liquid Fe, but the effect of the oxide phase could not be revealed in the present work. The elucidation of the removal mechanism in this region requires further examination.

Table 2 Binary interaction parameters, Ω, and the Gibbs' free energy of SiO_2 formation

	Values/J	Region of validity
${}^0\Omega_{Fe-O}$	$-415400 + 142.4T$	$X_O < 0.0040$, $1823 \leq T \leq 1973$
${}^1\Omega_{Fe-O}$	$298300 - 117.8T$	$X_O < 0.0040$, $1823 \leq T \leq 1973$
${}^0\Omega_{Fe-Si}$	$-343500 + 114.0T$	$X_{Si} < 0.080$, $1823 \leq T \leq 1973$
${}^1\Omega_{Fe-Si}$	$217200 - 100.1T$	$X_{Si} < 0.080$, $1823 \leq T \leq 1973$
Ω_{Si-O}	$479400 - 322.1T$	$X_{Si} < 0.080$, $X_O < 0.0040$, $1823 \leq T \leq 1973$
$\Delta G^\circ_{f,Si-O}$	$-946300 + 197.7T$	

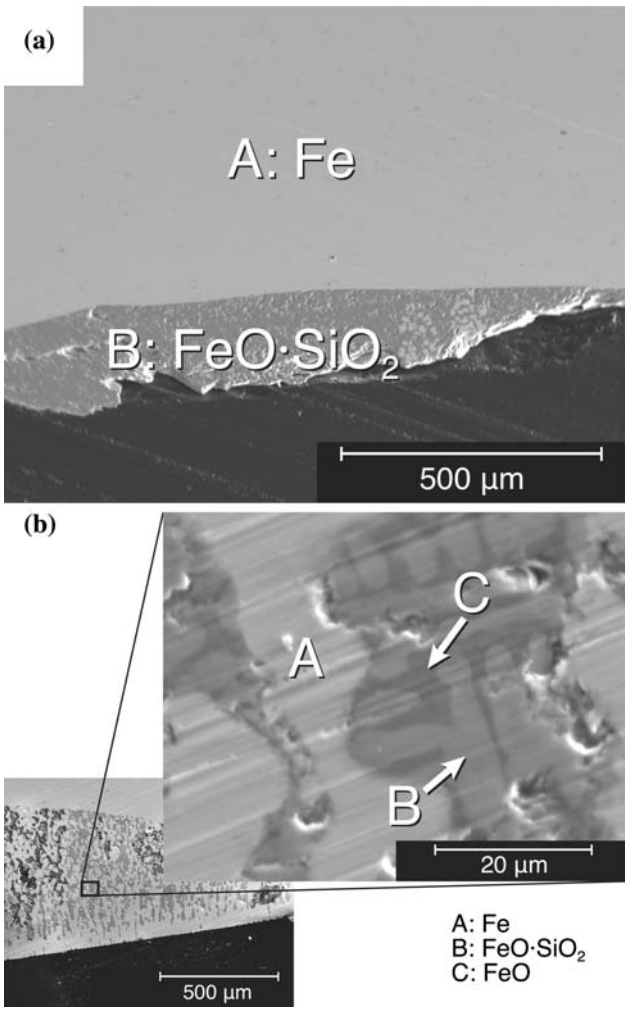

Fig. 6 The cross sectional SEM images of (**a**) black and (**b**) gray beads formed on the surface of specimens. Total melting time; (**a**) 2 min, (**b**) 40 min

Conclusions

It was confirmed that oxidation refining using PAM has an efficiency to remove some impurities from Fe and 99.93 mass% Fe was easily refined up to 99.996 mass%. Among these impurities, the removal of Si is caused by the redistribution of Si between in the Fe phase and in the oxide phase following the relationship of Si and oxygen in liquid Fe. And Si decreased to below 1 mass ppm when the initial concentration of Si was 7 ± 3 mass ppm. Although $Fe_{1-x}O$ seems to be attributed to this further elimination of Si, the function of $Fe_{1-x}O$ phase is unclear in the present work.

In addition, the purification of Fe by anion-exchange separation was reported by the present authors [28, 29]. We have succeeded in eliminating almost all metallic impurities from Fe but Si contamination was sometimes found. Although it is highly likely that the degree of Si contamination depends on the quality of water used in anion-exchange separation, the source of this contamination has not been identified clearly. So, the oxidation refining using PAM described in this paper is a very useful method to remove Si from high purity Fe refined by anion-exchange separation.

References

1. Powalla M, Herz K (1993) Appl Surf Sci 65/66:482
2. Ji SY, Lalev GM, Wang JF, Uchikoshi M, Isshiki M (2005) Mater Lett 59(18):2370
3. Abiko K (1997) Phys Status Sol (a) 160(2):285
4. Coze JL (2000) Mater Trans JIM 41(1):219
5. Kékesi T, Isshiki M (2002) The purification of base transition metals, chap. 3, pp. 71–101. Purification process and characterization of ultra high purity metals. Springer-Verlag Berlin Heidelberg New York
6. Mimura K, Nanjo M (1990) Mater Trans JIM 31(4):293
7. Mimura K, Saito K, Isshiki M (1999) J Jpn Inst Met 63(9):1181
8. Mimura K, Isshiki M (2002) Hydrogen plasma arc melting, chap. 6, pp. 181–202. Purification process and characterization of ultra high purity metals. Springer-Verlag Berlin Heidelberg New York
9. Mimura K, Lee S-W, Isshiki M (1995) J Alloy Compd 221(1–2): 267
10. Elanski D, Mimura K, Ito T, Isshiki M (1997) Mater Lett 30(1):1
11. Lim JW, Mimura K, Isshiki M (2005) J Mater Sci 40(15):4109. doi:10.1007/s10853-005-0642-7
12. Elanski D, Lim JW, Mimura K, Isshiki M (2006) J Alloy Compd 413(1–2):251
13. Elanski D, Lim JW, Mimura K, Isshiki M (2006) J Alloy Compd 421(1–2):209
14. Elanski D, Lim JW, Mimura K, Isshiki M (2007) J Alloy Compd 439(1–2):210
15. Dembovsky V (1998) J Mater Process Technol 78(1–3):36
16. Knacke O, Kubaschewski O, Hesselmann K (eds) (1991) Thermochemical properties of inorganic substances, vol 1 and 2, 2nd edn. Springer-Verlag, Berlin, New York
17. Hilty D, Crafts W (1950) Trans AIME 188:425
18. Gokcen NA, J Chipman (1952) J Met 4(2):171
19. Matoba S, Gunji K, Kuwana T (1959) Tetsu-to-Hagané 45(12):1328
20. Segawa K, Tsunetomi E, Nakamura Y, Chino H (1965) Tetsu-to-Hagané 51(10):1866
21. Suzuki K, Ban-ya S, Fuwa T (1970) Tetsu-to-Hagané 56(1):20
22. Tankins ES, Gokcen NA, Belton GR (1964) Trans Metall Soc AIME 230:820
23. TJS for Promotion of Science The 19th committee in steelmaking (1988) Steelmaking Data Sourcebook. Gordon and Breach Science Publishers, New York, NY
24. Miki T, Hino M (2004) ISIJ Int 44(11):1800
25. Miki T, Hino M (2005) ISIJ Int 45(12):1848
26. Chase JMW (eds) (1988) NIST-JANAF Thermochemical Tables, 4th edn. The American Chemical Society and The American Institute of Physics for the National Institute of Standards and Technology
27. Larson H, Chipman J (1953) Trans AIME 197:1089
28. Kekesi T, Mimura K, Isshiki M (2002) Hydrometallurgy 63(1):1
29. Uchikoshi M, Imaizumi J, Shibuya H, Kekesi T, Mimura K, Isshiki M (2004) Thin Solid Films 461(1):94